

The LBT Y_p Project I: An Improved Determination of the Primordial Helium Abundance – Project Description, Sample Selection, Observations, and Methodology

EVAN D. SKILLMAN,¹ RICHARD W. POGGE,^{2,3} ERIK AVER,⁴ NOAH S. J. ROGERS,⁵ MIQUELA K. WELLER,² KEITH A. OLIVE,⁶ DANIELLE A. BERG,⁷ JOHN J. SALZER,⁸ JOHN H. MILLER, JR.,¹ JAYDE SPIEGEL,^{2,9} TSUNG-HAN YEH,¹⁰ AND BRIAN D. FIELDS^{11,12,13}

¹*Minnesota Institute for Astrophysics, University of Minnesota, 116 Church St. SE, Minneapolis, MN 55455*

²*Department of Astronomy, The Ohio State University, 140 W 18th Ave., Columbus, OH, 43210*

³*Center for Cosmology & AstroParticle Physics, The Ohio State University, 191 West Woodruff Avenue, Columbus, OH 43210*

⁴*Department of Physics, Gonzaga University, 502 E Boone Ave., Spokane, WA, 99258*

⁵*Center for Interdisciplinary Exploration and Research in Astrophysics (CIERA), Northwestern University, 1800 Sherman Avenue, Evanston, IL 60201, USA*

⁶*William I. Fine Theoretical Physics Institute, School of Physics and Astronomy, University of Minnesota, Minneapolis, MN 55455, USA*

⁷*Department of Astronomy, The University of Texas at Austin, 2515 Speedway, Stop C1400, Austin, TX 78712, USA*

⁸*Department of Astronomy, Indiana University, 727 East Third Street, Bloomington, IN 47405, USA*

⁹*Department of Physics, University of California Santa Cruz, 1156 High Street, Santa Cruz, CA 95064*

¹⁰*TRIUMF, 4004 Wesbrook Mall, Vancouver, BC V6T 2A3, Canada*

¹¹*Department of Astronomy, University of Illinois, Urbana, IL 61801*

¹²*Department of Physics, University of Illinois, Urbana IL 61801*

¹³*Illinois Center for Advanced Studies of the Universe*

ABSTRACT

Extremely low metallicity H II regions have been observed with the goal of determining the primordial helium abundance (Y_p). Y_p , combined with standard big bang nucleosynthesis and the half-life of the neutron, provides a direct measurement of the number of neutrino families, but Y_p must be measured very precisely to provide meaningful constraints on physics beyond the Standard Model. Here we describe a program to combine new Large Binocular Telescope (LBT) observations with a new analysis methodology to significantly improve the determination of Y_p . The LBT, with its MODS and LUCI instruments, produces spectra, which, when combined with our new analysis methodology, are capable of delivering He abundances in individual H II regions with uncertainties of approximately 2% or less. Archival LBT/MODS spectra of standard stars over a four-year period enable the determination of a wavelength-dependent uncertainty in the MODS spectral response, resulting in improved relative emission line uncertainties. An optimized sample of low-metallicity galaxies has been selected with the goal of producing a determination of Y_p with a precision of $\sim 0.5\%$, sufficient to provide an independent constraint on the effective number of neutrino families of $\sim 3\%$.

Keywords: Chemical abundances (224), H II regions (694), Cosmic abundances(315), Big Bang nucleosynthesis(151), Infrared spectroscopy(2285), Spectroscopy(1558)

1. INTRODUCTION

The LBT Y_p Project is designed to produce a robust, high precision measurement of the primordial helium abundance (Y_p).

1.1. Project Motivation

Standard big bang nucleosynthesis (SBBN; K. A. Olive et al. 2000; F. Iocco et al. 2009; R. H. Cyburt et al. 2016; C. Pitrou et al. 2018; B. D. Fields et al. 2020) remains one of the deepest available probes to the early universe. It is also an important probe of physics beyond the Standard Model (S. Sarkar 1996; R. H. Cyburt et al. 2005; T.-H. Yeh et al. 2022;

K. Jedamzik & M. Pospelov 2009; M. Pospelov & J. Pradler 2010). New physics, which affects the idealized conditions of a radiation-dominated thermal bath at a temperature of roughly 1 MeV, has the potential of breaking the agreement between theory and the observational determinations of the ^4He and deuterium abundances. For example, theories which include new particle degrees of freedom lead to an increased rate of expansion during nucleosynthesis, leaving less time for the conversion of neutrons to protons, and hence lead to an increased helium mass fraction (G. Steigman et al. 1977; R. H. Cyburt et al. 2016; B. D. Fields et al. 2020; T.-H. Yeh et al. 2022). These new particle degrees of freedom are often

scaled as contributions to the number of very light neutrinos, N_ν . The upper limits on N_ν from BBN rely heavily on accurate measurements of the primordial helium abundance, Y_p .

Although the cosmic microwave background (CMB) measurements by *WMAP* (E. Komatsu et al. 2014) and *Planck* (Planck Collaboration et al. 2020) provide an unparalleled determination of the fundamental parameters of the standard cosmological model, including cold dark matter and dark energy (Λ CDM), big bang nucleosynthesis and the observations of the light element abundances also offer an important cross-check, in particular on the determination of the baryon density. The most recent *Planck* result for the baryon density (which takes into account the correlation between the baryon density and the helium abundance), $\Omega_B h^2 = 0.02237 \pm 0.00015$, corresponds to a baryon-to-photon ratio of $\eta = (6.12 \pm 0.04) \times 10^{-10}$. Because the uncertainty in η is now less than 1%, SBBN (defined with $N_\nu = 3$) has effectively become a parameter-free theory (R. H. Cyburt et al. 2002), and relatively precise predictions of the primordial abundances of the light elements D, ^3He , ^4He , and ^7Li are available (e.g., B. D. Fields et al. 2020). While the ^7Li abundance remains problematic (e.g., R. H. Cyburt et al. 2008; B. D. Fields & K. A. Olive 2022), D/H determinations from quasar absorption systems have become quite precise, and are in excellent agreement with the prediction from SBBN and the CMB (e.g., R. J. Cooke et al. 2014, 2016, 2018; S. Riemer-Sørensen et al. 2015, 2017; S. A. Balashev et al. 2016; E. O. Zavarygin et al. 2018; F. Guarneri et al. 2024; P. A. Kislytsyn et al. 2024).

Using a neutron mean life of 878.4 ± 0.5 s (S. Navas et al. 2024) and the *Planck* value of η , SBBN yields a primordial abundance for ^4He , $Y_p = 0.2467 \pm 0.0002$ (T.-H. Yeh et al. 2022, 2023). By allowing Y_p to vary as an independent parameter, fits to CMB anisotropies allow for a determination of Y_p within the context of Λ CDM. The recent *Planck* results found $Y_p = 0.239 \pm 0.013$ (68% CL) (Planck Collaboration et al. 2020). This 5.4% uncertainty on Y_p , from CMB measurements alone, is currently not competitive with other constraints; the helium abundance from emission line measurements from metal-poor galaxies provides significantly better precision, cf. $Y_p = 0.2448 \pm 0.0033$ (E. Aver et al. 2022), a 1.3% determination.

More recently, the Atacama Cosmology Telescope (ACT) has combined ground based measurement of the CMB at high multipoles with *Planck* data and Dark Energy Survey Instrument (DESI) Baryon Acoustic Oscillations (BAO) data to obtain $Y_p = 0.2312 \pm 0.0092$ (68% CL) - a 4% uncertainty (E. Calabrese et al. 2025). Similarly, the South Pole Telescope (SPT) has obtained $Y_p = 0.2285 \pm 0.0085$ (68% CL) when SPT data is combined with *Planck* and ACT data (E. Campagne et al. 2025). This is a 3.7% determination.

A precise primordial abundance is available not only for ^4He , but also for deuterium, which is measured via its Lyman lines in quasar absorption systems. The weighted mean over 12 systems gives $\text{D/H} = (2.513 \pm 0.028) \times 10^{-5}$. The SBBN prediction for D/H is $(2.506 \pm 0.083) \times 10^{-5}$ (T.-H. Yeh et al. 2023). For D/H, theory is lagging behind the precision of the observational data, primarily due to uncertainties in the nuclear cross sections for the $d(d, p)t$ and $d(d, n)^3\text{He}$ reactions. The agreement is nevertheless excellent.

To test SBBN beyond D/H, it is clear that precise determinations of ^4He are necessary. Since Y_p scales as $\eta^{0.04}$ in SBBN, it is unlikely that ^4He abundance measurements will ever be competitive with the CMB and/or D/H determinations in fixing the baryon density since D/H scales as $\eta^{-1.634}$ in SBBN (T.-H. Yeh et al. 2023). Although D/H also scales more strongly with N_ν (as $N_\nu^{0.405}$) as compared with ^4He (which scales as $N_\nu^{0.163}$), due to the uncertainties in the BBN predictions of D/H, Y_p provides the strongest constraints available on N_ν and hence on the physics of the early universe beyond the Standard Model (R. H. Cyburt et al. 2005; T.-H. Yeh et al. 2022). Currently, the combination of *Planck* CMB data with abundance measurements used in BBN has a maximum likelihood with $N_\nu = 2.898 \pm 0.141$, just below the Standard Model value of 3; the uncertainty in this value depends sensitively on the data considered (B. D. Fields et al. 2020; T.-H. Yeh et al. 2022). For example, the CMB alone can fix N_ν only with a precision of ± 0.29 (68% CL). However, when *Planck* data are combined with the BBN relation between Y_p and η , this uncertainty improves to ± 0.19 without using any abundance data. Current helium abundance data further improve the uncertainty to ± 0.15 , while D/H (without Y_p) gives ± 0.18 and is competitive with ^4He .

More recent CMB experiments find increased precision for the effective number of neutrinos at later epochs. In the Standard Model, $N_{\text{eff}} = 3.044$ (M. Drewes et al. 2024)¹⁴ and does not evolve between BBN and CMB decoupling. For example, ACT combined with *Planck* and DESI BAO obtain $N_{\text{eff}} = 2.86 \pm 0.13$ (E. Calabrese et al. 2025). SPT data combined with *Planck* and ACT give $N_{\text{eff}} = 2.81 \pm 0.12$ (E. Campagne et al. 2025). Indeed, it is hoped that future CMB missions can improve these uncertainties $< \pm 0.09$ for the CMB alone (K. Abazajian et al. 2019), and $< \pm 0.06$ when the CMB is combined with BBN and Y_p determinations (T.-H. Yeh et al. 2022). The primary goal of the LBT Y_p Project is to reduce the uncertainty on Y_p from 1.3% to $\sim 0.5\%$. This re-

¹⁴ N_{eff} , the effective number of neutrino flavors, is a measure of the total energy density of relativistic particles in the early universe. The Standard Model value for N_{eff} is slightly greater than the 3 Standard Model neutrino flavors due to the slightly higher temperature from e^+e^- annihilation before neutrinos are completely decoupled.

duction in the uncertainty in Y_p translates into an uncertainty on the number of neutrino families from 0.14 to ~ 0.08 .

An improvement in the uncertainty in N_ν of this magnitude will allow one to probe in detail the decoupling period prior to BBN. Ultimately, the goal of distinguishing between the Standard Model number of light neutrinos $N_\nu = 3$ and the effective number of neutrinos affecting the expansion rate of the Universe, $N_{\text{eff}} = 3.044$, seems within reach. Furthermore, barring a systematic shift in the maximum likelihood value for N_ν , the reduction in its uncertainty, or, equivalently, the uncertainty on N_{eff} , will place unprecedented constraints on physics beyond the Standard Model. Physics beyond the Standard Model may also induce a change in the effective number of degrees of freedom between BBN and CMB decoupling. This too, is an interesting challenge, perhaps also within reach.

As noted above, certain physics beyond the Standard model can affect the expansion rate of the Universe at the time of BBN. The expansion rate, characterized by the temperature-dependent Hubble parameter is primarily determined by the energy density in radiation (at the time of BBN),

$$H^2(T) \simeq \frac{8\pi}{3} G_N \rho_R, \quad (1)$$

where G_N is Newton's constant and, around the time of BBN,

$$\rho_R = \rho_\gamma + \rho_e + \rho_\nu = \frac{\pi^2}{30} \left(2 + \frac{7}{2} + \frac{7}{4} N_\nu \right) T^4. \quad (2)$$

Thus, new physics contributing to the energy density can be constrained by its effective contribution to N_ν . For example, in models of neutrino masses which involve light right-handed or sterile neutrinos, the interactions of these states must be weak enough so that they decouple long before Standard Model neutrino decoupling at $\simeq 2$ MeV, suppressing their temperature relative to the left-handed neutrinos and hence their contribution to N_ν . This may set lower limits to the mass of an extra gauge boson mediating right-handed interactions (see e.g. [G. Steigman et al. \(1986\)](#); [M. C. Gonzalez-Garcia & J. W. F. Valle \(1990\)](#); [V. Barger et al. \(2003\)](#)) or the degree of mixing between sterile neutrinos and left-handed neutrinos ([A. D. Dolgov & F. L. Villante 2004](#); [S. Böser et al. 2020](#); [G. Alonso-Álvarez & J. M. Cline 2022](#)). Similar limits would apply to any dark radiation present at the time of BBN or to a non-relativistic matter component ([N. Sabti et al. 2020](#); [T.-H. Yeh et al. 2024](#)). Other limits include constraints on primordial gravitational waves ([L. A. Boyle & A. Buonanno 2008](#); [K. Kohri & T. Terada 2018](#)).

Determinations of Y_p are also relevant to attempts to resolve the Hubble tension (e.g., [A. G. Riess et al. 2019, 2021](#)). In particular, BAO and BBN data (via primordial deuterium and helium abundances) allow for a CMB-independent determination of H_0 for comparison with distance ladder determinations ([G. E. Addison et al. 2018](#); [N. Schöneberg et al.](#)

[2019](#)). Furthermore, many models of new physics beyond the Standard Model proposed to resolve the Hubble tension often require increases in N_{eff} or are motivated in their design by limits on it. Correspondingly, limits on N_{eff} inferred from measurements of Y_p help constrain models of new physics proposed for resolving the Hubble tension. Prominent, outstanding questions in cosmology, such as the Hubble tension, and the range of extensions beyond the Standard Model which are constrained by BBN and the measurement of Y_p , demonstrate the importance of a better, higher precision determination of Y_p .

1.2. Present State of the Art

1.2.1. Recent Methodology Improvements

The most precise values of Y_p are determined by fitting the helium abundance versus a measurement of metallicity (e.g., oxygen) from HII regions, and extrapolating back to very low metallicity as first demonstrated by [M. Peimbert & S. Torres-Peimbert \(1974\)](#). Thus, improvements in the uncertainty on the extrapolation can come from reducing the uncertainties on individual measurements and by increasing the number of high-quality measurements. Historically, obtaining better than $\sim 3\%$ precision for individual objects has been a challenge. ^4He abundance determinations are vulnerable to systematic uncertainties and degeneracies among the input parameters needed to model emission line fluxes ([K. A. Olive & E. D. Skillman 2001, 2004](#); [V. Luridiana et al. 2003](#); [M. Peimbert et al. 2007](#); [Y. I. Izotov et al. 2007](#); [E. Aver et al. 2010](#)). Using Monte Carlo methods reveals these degeneracies, puts these determinations on a firm statistical basis, and allows an objective comparison between data and theoretical models ([E. Aver et al. 2011, 2012](#)). Curiously, [E. Aver et al. \(2012\)](#) discovered that, in many cases, the models used to extract abundances are statistically inconsistent with the observations (in that those solutions fail to pass a standard 95% CL χ^2 test) and employed corresponding quality cuts on their dataset. Subsequent analyses by other groups adopting the [E. Aver et al. \(2012\)](#) methodology found similar inconsistencies ([V. Fernández et al. 2019](#); [T. Hsyu et al. 2020](#)), and others have employed stringent cuts on their observational data for related reliability concerns ([Y. I. Izotov et al. 2013, 2014](#)). Our recent research is consistent with the hypothesis that these incompatibilities are primarily due to deficiencies in the observations. In particular, note that many of these observations are now quite old – the majority of the analyzed targets come from the HeBCD dataset, with observations dating back to the 1990s ([Y. I. Izotov et al. 2007](#)). Using higher quality, higher spectral resolution, broader wavelength coverage observations has generally produced statistically consistent model solutions.

For example, [E. Aver et al. \(2012\)](#) started with a dataset of 93 observations of 86 HII regions in 77 galaxies from

[Y. I. Izotov et al. \(2007\)](#). It was argued that the absence of He I $\lambda 4026$ in 23 of the observations led to a systematic bias towards higher ${}^4\text{He}$, and those observations without $\lambda 4026$ were discarded. However, analysis of the remaining 70 observations, found that, in 45 of them, the comparison between model and data resulted in $\chi^2 > 4$, thus indicating a poor model fit to the data at the 95.45% CL, given nine observed line ratios and eight model parameters used in that model. Further cuts were made due to solutions with very high ($> 25\%$) neutral hydrogen fraction, or very high oxygen abundances, leaving 22 observations, of which eight were flagged with either a large optical depth or large underlying absorption in either H or He. Thus, the vast majority of the observations were deemed unsuitable for further analysis. In fact, when [E. Aver et al. \(2013\)](#) used improved emissivities from [R. L. Porter et al. \(2012, 2013\)](#) to calculate a revised value of Y_p , the solutions for only two objects improved to an acceptable level giving a total of 16 observations to deduce Y_p , indicating that inaccuracies in emissivities were likely *not* the dominant cause of statistically inconsistent solutions for targets.

A significant breakthrough came with the addition of observations of the NIR He I $\lambda 10830$ emission line, as first suggested by [Y. I. Izotov et al. \(2014\)](#), which led to significant improvements in the ${}^4\text{He}$ abundance determinations ([Y. I. Izotov et al. 2014; E. Aver et al. 2015](#)). The He I $\lambda 10830$ line is particularly useful as it helps break some of the degeneracies in the parameters used to derive the ${}^4\text{He}$ abundance, most notably that between the electron density, n_e , and temperature, as highlighted by [E. Aver et al. \(2010\)](#). For example, 31 targets from [Y. I. Izotov et al. \(2007\)](#) contained He I $\lambda 10830$ observations ([Y. I. Izotov et al. 2014](#)), and these were subject to the MCMC analysis now with ten flux ratios to fit the same eight parameters. Without He I $\lambda 10830$, only 11 of the 31 objects survived the various cuts employed. With He I $\lambda 10830$, that total grew to 16 (though two corresponded to independent observations of the same galaxy). This result strongly highlights the benefits of expanding the model to employ additional observations.

In a study of the extremely metal poor object Leo P, [E. Aver et al. \(2021\)](#) demonstrated that taking advantage of the large wavelength baseline of LBT/MODS enables the use of additional hydrogen and helium emission lines and results in better constrained model parameters, particularly the reddening. Additional improvements were made to the treatment of the collisional excitation of H I. After the required addition of collisional excitation rates to higher levels, adding more hydrogen emission lines provided a better constraint on the impact of the collisional excitation. The correction for underlying stellar absorption was revisited, and through the use of BPASS stellar evolution and spectral synthesis models of [J. J. Eldridge & E. R. Stanway \(2009\)](#); [E. R. Stanway & J. J. Eldridge \(2018\)](#), a uniform set of scaling relations was developed to include all of the newly added hydrogen and helium emission lines. [E. Aver et al. \(2021\)](#) also revisited the procedure for handling the blended line He I $\lambda 3889$ with H8, including its underlying absorption and radiative transfer.

[O. A. Kurichin et al. \(2021a\); O. A. Kurichin & A. V. Ivanchik \(2024\); O. Kurichin & A. Ivanchik \(2025\)](#) represent a series of suggested improvements in the methodology for deriving Y_p . [O. A. Kurichin et al. \(2021a\)](#) addresses the often used method of deriving the value of O/H when only one measurement of temperature is available. Typically, the temperature in the high ionization zone derived from O III observations is used to infer a temperature in the low ionization zone, and [O. A. Kurichin et al. \(2021a\)](#) point out that the inferred low ionization zone temperature can be biased and its uncertainty can be underestimated (as noted previously in other contexts by, e.g., [K. Z. Arellano-Córdova & M. Rodríguez 2020](#); [N. S. J. Rogers et al. 2021, 2022](#)). As a result, O^+/H^+ can be biased, resulting in a biased measurement of O/H. In the LBT Y_p project, we obtain multiple direct temperature measurements which allow us to make a better estimate of the appropriate temperature for the low ionization zone and its uncertainty.

[O. A. Kurichin & A. V. Ivanchik \(2024\)](#) present a suggested improvement for the treatment of the underlying absorption in the H I and He I lines. In brief, they model the underlying absorption based on full SED-fitting of the observed galaxy spectrum, including stellar and nebular continua as well as emission-line profiles. This is claimed to be superior to the methodology of, e.g., [E. Aver et al. \(2021\)](#), which scales the equivalent widths of individual lines based on numerical studies of the emission lines in single stellar populations (e.g., [J. J. Eldridge et al. 2017](#); [E. R. Stanway & J. J. Eldridge 2018](#)). We have not been able to test and compare these techniques, but we do note that our modeling of underlying absorption produces very reasonable minimization values.

[O. Kurichin & A. Ivanchik \(2025\)](#) produce a new grid of He I radiative transfer corrections. This grid is consistent with modern He I emissivities and identifies flaws in the previously used corrections ([R. A. Benjamin et al. 2002](#)). We greatly appreciate this new contribution and we have adopted these radiative transfer corrections for the LBT Y_p project.

1.2.2. Recent Results

Fig. 1 gives a visual representation of recent determinations of Y_p , listed in chronological order and compared to the SBBN result based on the Planck determined baryon density ([T.-H. Yeh et al. 2022](#)). All of the points were determined through observations of HII regions in metal-poor galaxies except for the [R. J. Cooke & M. Fumagalli \(2018\)](#) point, from observations of an absorption system, and three deter-

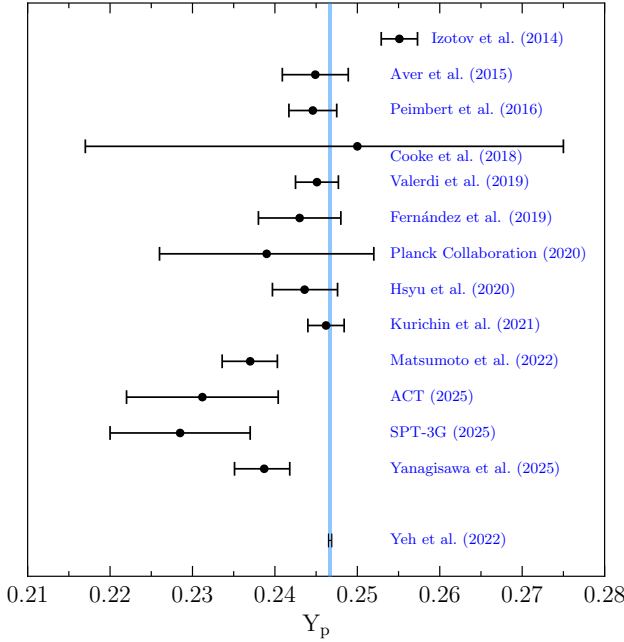


Figure 1. A comparison of recent Y_p results. The SBBN result based on the Planck determined baryon density [Planck Collaboration et al. \(2020\)](#) is plotted as a vertical band in light blue (T.-H. Yeh et al. 2022, 2023).

minations based on CMB observations ([Planck Collaboration et al. 2020](#); [E. Calabrese et al. 2025](#); [E. Camphuis et al. 2025](#)) as described earlier in Section 1.1. In this subsection, we will described the determinations based on H II region observations in more detail.

[E. Aver et al. \(2015\)](#) derived a value of $Y_p = 0.2449 \pm 0.0040$ from a sample of 15 objects which passed the χ^2 cut-off. This value was in tension with with value of $Y_p = 0.2551 \pm 0.0022$ previously derived by [Y. I. Izotov et al. \(2014\)](#). While both analyses were drawn from the same observational database, the analysis methodologies and samples were different. [Y. I. Izotov et al. \(2014\)](#) emphasized that their result corresponded to a value of $N_{\text{eff}} = 3.58 \pm 0.25$, implying a significant departure from the Standard Model. The value from [E. Aver et al. \(2015\)](#) is consistent with SBBN.

These studies were closely followed by others. [A. Peimbert et al. \(2016\)](#) used observations of five objects and an assumed slope of $\Delta Y / \Delta O = 3.3 \pm 0.7$ to derive $Y_p = 0.2446 \pm 0.0029$. In a similar approach, [M. Valerdi et al. \(2019\)](#) combined a very precise measurement of He/H in the Small Magellanic Cloud H II region NGC 346 with the same assumed slope of $\Delta Y / \Delta O$ to obtain a value of $Y_p = 0.2451 \pm 0.0026$. The more recent analysis of [V. Fernández et al. \(2018\)](#), using SDSS-III data with regressions in O/H, N/H, and S/H, found $Y_p = 0.245 \pm 0.007$, which improved to $Y_p = 0.243 \pm 0.005$, when Bayesian statistical techniques were applied ([V. Fernández et al. 2019](#)). [V. Fernández et al. \(2018\)](#) use the collin-

sionally excited [S III] lines to derive a nebular temperature, and this appears to be a good choice for H II regions where the quality of the spectra does not allow a measurement of the temperature from the He I lines (as opposed to a temperature measurement from the [O III] lines which may be more strongly biased toward higher temperatures). All four of these independent analyses agree with the result of [E. Aver et al. \(2015\)](#) within the limits of their uncertainties.

[T. Hsyu et al. \(2020\)](#) presented new Keck NIRSPEC and NIRES Keck observations of He I $\lambda 10830$ in 16 galaxies identified from SDSS imaging and having existing optical spectra ([T. Hsyu et al. 2018](#)). Their analysis followed the [E. Aver et al. \(2015\)](#) model, and, in their primary data sample, they combined their new observations with 13 targets from the HeBCD sample and 38 targets from the Sloan Digital Sky Survey (SDSS). From the combined dataset they obtained $Y_p = 0.2436^{+0.0039}_{-0.0040}$ in good agreement with [E. Aver et al. \(2015\)](#). Importantly, [T. Hsyu et al. \(2020\)](#) highlight the fact that only a small fraction of their newly observed targets (3 targets in their primary sample) passed their quality cuts for successful modeling and noted that their highest quality spectra were the most likely to pass. While [T. Hsyu et al. \(2020\)](#) followed the [E. Aver et al. \(2015\)](#) model, there are important differences that are discussed in Appendix A.

This has been followed by [O. A. Kurichin et al. \(2021b\)](#), who employed the [E. Aver et al. \(2015\)](#) model and methodology on 100 spectra from the SDSS, combined with 20 spectra from the HeBCD database. Their resulting measurement of Y_p is consistent with the results of [E. Aver et al. \(2015\)](#) and [T. Hsyu et al. \(2020\)](#), but with an uncertainty reduced by almost a factor of two. We have some concerns about the [O. A. Kurichin et al. \(2021b\)](#) sample since it is dominated by SDSS spectra, which tend to be quite low SNR. Furthermore, the SDSS spectra used by [T. Hsyu et al. \(2020\)](#) and [O. A. Kurichin et al. \(2021b\)](#) are dominantly at higher metallicities ($O/H \geq 8 \times 10^{-4}$) and generally have larger uncertainties (typically larger than 5%, in part, reflecting the absence of He I $\lambda 10830$ measurements). Nonetheless, the uncertainty on Y_p is reduced simply due to the large number of targets.

It is our opinion that adding large numbers of low quality points, while statistically effective, is not the best path forward. In a discussion of how best to improve the measurement of Y_p , [G. J. Ferland et al. \(2010\)](#) provide several arguments as to why it is better to use exclusively high quality spectra. The SDSS spectra reduce the uncertainty on Y_p primarily by reducing the uncertainty on the slope of the Y versus O/H relationship. This increases the vulnerability to the assumption of a perfectly linear relationship, which is not necessarily to be expected given the different nucleosynthetic origins of helium and oxygen (or nitrogen or sulfur). Additionally, at high metallicity, our methodology cannot strongly constrain the neutral hydrogen fraction (because

it is determined through the collisional excitation of neutral hydrogen, which decreases precipitously with lower temperatures), although, at these low temperatures, this correction should be negligible. Nonetheless, objects at higher metallicity have the potential for an additional systematic uncertainty. Finally, the uncertainty in the mean can be underestimated if the dispersion is too large (see discussion in Paper IV).

Importantly, [O. A. Kurichin et al. \(2021b\)](#) conducted a reanalysis of the [Y. I. Izotov et al. \(2014\)](#) study. They identified three items in the [Y. I. Izotov et al. \(2014\)](#) analysis which they called into doubt: the dropping of λ 3889 and λ 7075; assuming a value for the He I underlying absorption; and applying a hard prior in a limited range for the temperature based on T[O III]. [O. A. Kurichin et al. \(2021b\)](#) duplicated the results of [Y. I. Izotov et al. \(2014\)](#), and then conducted a reanalysis without the three identified methodology concerns, and found a resulting value of Y_p in good agreement with SBBN.

[A. Matsumoto et al. \(2022\)](#) added new He I λ 10830 observations of 10 extremely metal poor galaxies and used the [T. Hsyu et al. \(2020\)](#) methodology to derive their helium abundances. Of these ten galaxies, the solutions from the MCMC code for five did not pass the χ^2 criteria. For the five that did qualify, intriguingly, the solutions for density, underlying stellar absorption equivalent width, and optical depth produced negative values (of parameters that are intrinsically positive). The non-physical nature of these solutions were not addressed. These five newly observed targets were added to 54 objects from [T. Hsyu et al. \(2020\)](#) (only 8 of which have NIR spectroscopy) with metallicities reaching up to 40% of the solar value to derive $Y_p = 0.2370_{-0.0034}^{+0.0033}$. [A. Matsumoto et al. \(2022\)](#) emphasize that their result is 1σ lower than the value of [E. Aver et al. \(2015\)](#) and the following studies in agreement with that value. [A. Matsumoto et al. \(2022\)](#) note that, in a reanalysis of the [T. Hsyu et al. \(2020\)](#) observations, they obtain a nearly identical result and thus attribute the lower value of Y_p to the addition of the five newly observed extremely metal-poor (XMP) galaxies.

This study has recently been followed up by [H. Yanagisawa et al. \(2025\)](#). They add new NIR observations of 29 galaxies and combine these new observations with optical observations from the SDSS, Magellan, or literature sources. Of these 29, 15 galaxies do not pass a quality of fit criterion, 3 galaxies are dropped due to radiation softness, and 3 galaxies are dropped due to high N/O with a result that 10 pass their quality criteria. These 10 are added to 58 galaxies from the [A. Matsumoto et al. \(2022\)](#) study producing a Y_p slightly higher than that derived by [A. Matsumoto et al. \(2022\)](#), but within 1σ .

There are clear differences in the methodologies, observations, and results of the various literature studies. Thus, it is highly desirable to address these potential systematic uncertainties with a large dataset, at low metallicities, that is uni-

formly observed and analyzed for the purpose of measuring Y_p .

1.3. Overview of the Project Papers

This project will be presented in six papers. This paper (Paper I) consists of introductory material (§1), descriptions of the sample and observations (§2, 3), a discussion of new H and He emissivities (§4), a description of the project database (§5), and a summary (§6). Paper II ([N. Rogers et al. 2026](#)) describes the new LBT MODS observations, the derived physical conditions, and the O/H abundances for the sample. Paper III ([M. Weller et al. 2026](#)) describes the LBT LUCI near-IR observations and the $(\text{He I } \lambda 10380)/(\text{H I } \text{P}\gamma)$ ratio critical for constraining the density. Paper IV ([E. Aver et al. 2026](#)) describes our improved methodology, the resulting He abundance measurements, and our new derivation of Y_p . Paper V ([T.-H. Yeh et al. 2026](#)) presents calculations of the impact that our new derivation of Y_p has on the constraint on N_ν and, consequently, new physics. Paper VI (N. Rogers et al., in prep.) presents additional chemical abundance measurements, which are not directly involved in the determination of Y_p , but are an additional important result of our high quality optical spectra. Paper VI also provides access to all of the reduced data products.

2. SAMPLE SELECTION

2.1. New Discoveries of Low Metallicity Galaxies

Beyond our demonstrated model improvements, we are currently statistics limited. Clearly, enlarging the sample of XMP galaxies¹⁵, with well-determined He abundances, will lead to improved constraints on the value of Y_p . The XMP galaxies are the most relevant for measurements constraining Y_p ; however, historically, the searches for these galaxies have had very low yields (see discussion in [J. Sánchez Almeida et al. 2017](#)). Fortunately, in recent years, there have been a number of discoveries of XMP galaxies (e.g., [A. S. Hirschauer et al. 2016](#); [H. Yang et al. 2017](#); [N. G. Guseva et al. 2017](#); [T. Hsyu et al. 2017, 2018](#); [Y. I. Izotov et al. 2018, 2019](#); [P. Senchyna & D. P. Stark 2019](#); [S. A. Pustilnik et al. 2020, 2021](#); [T. Kojima et al. 2020, 2021](#)).

Although many of these XMP galaxies are too low in emission line surface brightness to be viable for precise He abundance measurements, observations of the most promising of these galaxies, with quality comparable to the observations of Leo P ([E. Aver et al. 2021](#)), represents a very desirable goal. In this regard, the DESI survey is especially promising. From

¹⁵ Here we adopt the definition of an XMP galaxy as having $12 + \log(\text{O/H}) \leq 7.35$ ([N. G. Guseva et al. 2015](#); [K. B. W. McQuinn et al. 2020](#)). Note that not all of the targets in our sample are this metal-poor, but the most metal-poor targets are most desirable because they reduce the vulnerability to the assumption of a linear relationship between He/H and O/H.

the early release observations, [H. Zou et al. \(2024\)](#) and [I. A. Zinchenko et al. \(2024\)](#) report numerous XMP galaxy discoveries, and recently [D. Scholte et al. \(2026\)](#) have produced a catalog of thousands of metal-poor star forming galaxies from the DESI Data Release 2. Although many of these fail our sample selection criteria (see next subsection), there is potential to significantly improve the sample of suitable, lowest metallicity targets.

2.2. The LBT Y_p Project Sample Criteria

Over the course of this project we have established criteria which optimize the utility of various targets for use in determining Y_p . First and foremost, we prioritize the lowest metallicity targets as judged by measurements of their oxygen abundance. With this choice, we are minimizing the impact of higher metallicity objects on our final determination of Y_p . Thus, we are prioritizing the measurement of Y_p over the measurement of $\Delta Y/\Delta O$. This has not necessarily been the case in previous Y_p measurements. For example, as an extreme case, [M. Valerdi et al. \(2019\)](#) make a determination of Y_p using observations of a single HII region in the SMC and a choice for the value of $\Delta Y/\Delta O$. It is our intention to have as little dependence on $\Delta Y/\Delta O$ as possible. This is primarily because, although all evidence to date supports it, assuming a strictly linear relationship between He/H and O/H (or N/H or S/H) implies an unquantifiable systematic uncertainty ([L. S. Pilyugin 1993](#); [B. D. Fields & K. A. Olive 1998](#)). If our entire sample consisted of targets with sufficiently low O/H such that the uncertainty in $\Delta Y/\Delta O$ were irrelevant, then a straightforward weighted average of the points, with no dependence on $\Delta Y/\Delta O$, would be the best possible path to a secure measurement of Y_p . Up to now, the number of XMP galaxies which meet our other criteria was not sufficient to put us in this regime. This work is an important step towards that goal.

Second, we prioritize sources with high emission-line fluxes. In order to strongly constrain the parameters which determine He/H (e.g., temperature, density, reddening, optical depth, underlying absorption, neutral fraction), we require high S/N in many intrinsically weak emission lines. In the end, we are seeking uncertainties in the helium abundances for individual targets of $\sim 3\%$ or less. Thus, high fluxes are a requirement. Experimentally, we have determined that targets with $H\beta$ fluxes above 10^{-15} erg s $^{-1}$ cm $^{-2}$ are required. For example, the Leoncino dwarf galaxy ([E. Aver et al. 2022](#)) with an $H\beta$ flux of 9×10^{-16} erg s $^{-1}$ cm $^{-2}$ does not produce uncertainties on He/H as low as we desire (although we retain it in our sample). On the other hand, Leo P ([E. Aver et al. 2021](#)), with an $H\beta$ flux of 3×10^{-15} erg s $^{-1}$ cm $^{-2}$ achieves a desirable uncertainty.

Finally, we prioritize sources with high emission line equivalent widths and have determined a guideline in $H\beta$

equivalent width. Even if a target has a sufficiently high $H\beta$ flux, if the continuum is strong, the weak emission lines will be lost to the random fluctuations in the continuum. Experimentally, we have determined that a target requires an $H\beta$ equivalent width ≥ 100 Å. The $F(H\beta)$ and $EW(H\beta)$ goals developed for the project were based on our experience with the accumulating LBT observations, but since the subsequent targets were chosen based on literature values, not all of the observed targets met these goals. It follows that those at higher metallicity or having less constrained values of He/H are less useful to the determination of Y_p .

A complete listing of our LBT observations is given in Table 1. This table lists the target name, coordinates, redshift, and the MODS and LUCI integration times. The tabulated integration times represent the total observing time for one LBT instrument, i.e., if a binocular observation lasted one hour, the table gives an integration time of 120 minutes. For the targets without LUCI integration times, it was determined from some feature(s) of their MODS observations that these are not viable targets. The final column provides notes, e.g., alternate target names, whether the MODS spectrum came from the archive, if the target is not viable Table 1 therefore lists all of the observations, some of which are not used in the final Y_p determination. The complete final sample is presented in paper IV.

3. OBSERVATIONS

3.1. Optical Spectroscopy

The LBT Y_p project utilizes the Multi-Object Double Spectrographs (MODS, [R. W. Pogge et al. 2010](#)) on the Large Binocular Telescope (LBT, [J. M. Hill 2010](#)) to obtain the optical spectra of H II regions in metal-poor galaxies. The MODS blue channel has a wavelength coverage of 3200–5700 Å and $R \sim 1850$ for the G400L (400 lines mm $^{-1}$) grating; the red channel has a wavelength range of 5500–10000 Å and $R \sim 2300$ for the G670L (250 lines mm $^{-1}$) grating. In combination, these spectrographs cover the full optical band and extend into the NIR at sufficient resolution for direct abundance analysis. A longslit mask of 1-arcsec width and 1-arcminute length is used as the target objects are typically not very extended, but even for extended objects, this slit provides adequate spatial coverage for accurate sky subtraction. The combination of sensitivity, resolution, and wavelength coverage of MODS permits high-quality optical spectroscopy for precise He/H measurements.

3.1.1. Observing Strategy

The airmasses of the observations varied depending on the time of observation, and, because the MODS spectrographs do not have atmospheric dispersion correctors, the celestial position angle of the slit was chosen to be the parallactic angle at mid-visit to minimize flux losses due to differential at-

Table 1. LBT Observations for the LBT Y_p Project

Object	R.A.	Decl.	z	Int. Time (min)		Other Names(s)/Notes
	(hh:mm:ss)	(deg:mm:ss)		MODS	LUCI	
AGC 198691	09:43:32.38	+33:26:57.9	0.0017	120	Literature	Leoncino, Previously Reported
DDO 68	09:56:46.80	+28:50:10.9	0.0017	160	160	UGC 5340
DESI J092331.28+645111.3	09:23:31.27	+64:51:11.3	0.0054	120	...	Not Viable
HS 0029+1748	00:32:03.11	+18:04:46.1	0.0071	60	60	
HS 0122+0743	01:25:34.20	+07:59:24.0	0.0098	60	60	UGC 993
HS 0134+3415	01:37:13.80	+34:31:12.0	0.0195	120	60	
HS 0811+4913	08:14:47.53	+49:04:00.7	0.0018	120	60	SHOC 193b
HS 0837+4717	08:40:29.91	+47:07:10.2	0.0420	60	Literature	SHOC 220
HS 1028+3843	10:31:51.63	+38:28:08.4	0.0295	60	120	
HS 1222+3741	12:24:36.72	+37:24:36.6	0.0404	120	120	
HS 1353+4706	13:55:25.66	+46:51:51.3	0.0281	120	120	
HS 1442+4250	14:44:11.48	+42:37:35.9	0.0021	60	120	UGC 9497
HS 2236+1344	22:38:31.12	+14:00:29.8	0.0206	80	60	
HSC J2314+0154	23:14:37.55	+01:54:14.3	0.0327	80	...	
I Zw 18 NW	09:34:02.17	+55:14:27.4	0.0025	120	...	Archival MODS
I Zw 18 SE	09:34:01.97	+55:14:28.2	0.0025	120	90	
J0118+3512	01:18:40.00	+35:12:57.0	0.0154	120	Literature	
J0519+0007	05:19:02.64	+00:07:23.0	0.0444	120	Literature	
J2213+1722	22:13:48.45	+17:22:35.6	0.0048	120	Literature	
KKH 46	09:08:36.54	+05:17:27.0	0.0021	80	...	Not Viable
KUG 0743+513	07:47:33.18	+51:11:24.8	0.0014	120	120	
KUG 1138+327	11:41:07.49	+32:25:37.2	0.0060	60	120	LEDA 36252, Archival MODS
LEDA 101527	15:09:34.17	+37:31:46.1	0.0326	160	80	
LEDA 2790884	08:25:55.52	+35:32:32.0	0.0020	120	Literature	
Leo P	10:21:45.10	+18:05:17.1	0.0009	45	120	AGC 208583, Previously Reported
Mrk 5	06:42:15.26	+75:37:30.4	0.0016	120	60	UGCA 130
Mrk 36	11:04:58.54	+29:08:15.7	0.0022	60	Literature	UGCA 225, Archival MODS
Mrk 71	07:28:42.80	+69:11:21.0	0.0004	60	60	NGC 2363A
SBS 0335-052E	03:37:44.06	-05:02:40.2	0.0135	120	120	
SBS 0926+606	09:30:09.05	+60:28:05.4	0.0138	120	60	LEDA 26955
SBS 0940+544	09:44:16.61	+54:11:34.3	0.0054	60	Literature	
SBS 0946+558	09:49:30.30	+55:34:47.0	0.0052	120	60	Mrk 22
SBS 0948+532	09:51:31.77	+52:59:36.0	0.0462	120	60	LEDA 28398
SBS 1030+583	10:34:10.15	+58:03:49.1	0.0075	60	Literature	Mrk 1434, Archival MODS
SBS 1135+581	11:38:35.68	+57:52:27.3	0.0032	120	Literature	Mrk 1450
SBS 1152+579	11:55:28.34	+57:39:52.0	0.0173	120	Literature	Mrk 193
SBS 1159+545	12:02:02.37	+54:15:49.6	0.0120	120	120	LEDA 2815986
SBS 1211+540	12:14:02.48	+53:45:17.4	0.0031	60	120	
SBS 1249+493	12:51:52.50	+49:03:27.7	0.0243	120	120	
SBS 1331+493	13:33:23.84	+49:06:12.8	0.0020	120	120	
SBS 1415+437	14:17:01.41	+43:30:05.5	0.0021	60	120	
SBS 1420+544	14:22:38.85	+54:14:09.2	0.0206	120	120	
SBS 1437+370	14:39:05.47	+36:48:21.0	0.0019	60	Literature	Mrk 475
SDSS J013352.55+134209.5	01:33:52.56	+13:42:09.4	0.0088	120	120	
SDSS J080758.0+341439.3	08:07:58.00	+34:14:39.3	0.0225	120	60	
SDSS J114827.33+254611.7	11:48:27.34	+25:46:11.8	0.0451	120	120	Archival MODS
SDSS J210455.31-003522.2	21:04:55.31	-00:35:22.2	0.0048	60	100	
SHOC 113	02:18:52.91	-09:12:18.8	0.0127	120	120	Not Viable
SHOC 133	02:40:52.21	-08:28:27.4	0.0822	60	...	
SHOC 357	12:01:22.31	+02:11:08.4	0.0033	...	120	LEDA 3120683
UGC 4483	08:37:03.08	+69:46:50.3	0.0005	60	120	
UGC 5541	10:16:53.12	+58:23:40.3	0.0078	120	120	
UGC 6456	11:28:00.97	+78:59:28.3	-0.0003	120	120	
UM 133	01:44:41.28	+04:53:26.0	0.0054	120	60	
UM 161	23:27:43.69	-02:00:55.9	0.0181	60	120	
UM 420	02:20:54.51	+00:33:23.6	0.0584	120	60	SBS 0218+003
UM 461	11:51:33.35	-02:22:21.9	0.0035	120	120	
UM 570	13:23:47.46	-01:32:52.0	0.0225	120	120	SHOC 424, Archival MODS
VCC 1744	12:38:06.89	+10:09:56.0	0.0038	120	120	LEDA 42204
WISEA J085115.60+584055.7	08:51:15.65	+58:40:55.0	0.0919	120	60	
WISEA J104457.84+035312.9	10:44:57.79	+03:53:13.2	0.0130	90	120	Archival MODS
WISEA J113623.81+470928.9	11:36:23.82	+47:09:29.1	0.0102	120	120	
WISEA J120503.54+455151.0	12:05:03.55	+45:51:50.9	0.0654	120	...	
WISEA J132723.31+402203.5	13:27:23.29	+40:22:04.2	0.0105	160	120	
WISEA J133126.86+415148.5	13:31:26.91	+41:51:48.3	0.0117	120	120	
WISEA J231048.92-021105.9	23:10:48.84	-02:11:05.7	0.0125	120	120	

mospheric refraction (A. V. Filippenko 1982) (MODS guide with a red filter with central wavelength of 660 nm, so slit losses due to refraction would mostly impact the blue end of the spectra). We further restricted the observing windows for each target to airmass less than 1.5 (elevation $> 42^\circ$), and for those objects that pass within 5-degrees of zenith at the LBT, we avoid observing windows where the target would pass into elevations where the telescope instrument rotator must work near its maximum tracking rate (LBT is an alt-az telescope). Observations were taken when seeing was $< 1.1''$, but we got acceptable spectra of compact targets in variable seeing conditions that exceeded this limit. Because observing time among the LBT members is allocated in week-long blocks that are queue scheduled, we were able to observe most of our planned targets over the course of the 3-year primary observing campaign with minimal weather losses.

In total, we obtained new, high-quality MODS optical spectra of 56 targets for a total of 70 hours (wall clock time) of LBT time (including overheads). In addition, we reduced and analyzed MODS spectra of 7 other targets taken from the LBT data archive, and we include our previous MODS observations of Leo P (E. Aver et al. 2021) and AGC 198691 (E. Aver et al. 2022).

Each new target was observed for 1-hour of open-shutter integration time with both MODS spectrographs identically configured, divided into three 20-minute exposures to allow clean removal of cosmic ray events from the raw images. A few targets could only be observed with one of the MODS spectrographs because the adaptive secondary mirror was unavailable on the other “eye” of the LBT. The goal was to obtain a sample where all targets were observed as homogeneously as possible with a ground-based telescope. Standard calibrations, flat fields, wavelength comparison lamps, and spectrophotometric standard stars, were obtained during each observing run.

3.1.2. Spectral Calibration

Because the LBT has a small facility instrument suite that is mounted on the telescope essentially all of the time, except for during summer shutdown, calibrations are very stable, as instruments are rarely disturbed. All regular calibrations for all LBT observing programs are released immediately on the LBT Observatory Data Archive¹⁶, so we can examine all available calibration data, not just those obtained as part of our observing campaign, and get a long-term quantitative assessment of the overall quality of the flux calibration of MODS. Further, one of the authors (RWP) was the MODS project lead and had established a long-standing cross-partner calibration program whereby the same calibration procedures were followed for all internal instrumental

calibrations (flat fields, wavelength calibration lamps, and biases) and flux standard star observations, so a high degree of calibration uniformity was maintained over many years before and after our campaign.

For our observations in our previous two Y_p studies (E. Aver et al. 2021, 2022), a uniform, wavelength-independent flux calibration uncertainty of 2% was assumed for all emission line measurements, based on the flux uncertainty quoted for the observations of standard stars (J. B. Oke 1990). This was a very conservative assumption (clearly two emission lines which are near to each other in wavelength will have a much smaller minimum uncertainty in their relative fluxes). With the new observations from the LBT Y_p Project, we could revisit this assumption and replace it with a new, wavelength dependent calibration uncertainty.

To derive MODS spectral response functions, we only used the best quality spectra of two HST CALSPEC (R. C. Bohlin et al. 2014) primary flux calibrator DA white dwarf stars, G191B2b and GD153 (R. C. Bohlin et al. 2019). Both stars had overlap between the observing semesters and were the highest priority flux stars in the overall observatory calibration program for MODS. Each star is observed with a special 5x60-arcsec calibration slit mask to eliminate seeing- and refraction-dependent slit losses. We restricted attention to observations of these stars in the LBT Archive from 2021 through 2024 that covered our campaign, and we reduced all the spectra starting from the raw data using our version of the modIDL pipeline¹⁷ to make 1D extracted spectra, and then calculated response curves including atmospheric extinction using a custom Jupyter notebook. Poor-quality spectra taken through clouds or with other issues were culled from the final sample. In total, our final sample consisted of 50 spectra of G191B2b and 19 spectra of GD153.

The historical response curves show the expected random changes in flux calibration due to weather; conditions at Mt. Graham are rarely photometric, but we see a well-defined upper envelop when it was photometric. Long-term trends seen in the LBT+MODS total throughput are understood as the accumulation of dust on the LBT primary mirrors and slow degradation of the exposed aluminum coatings. The LBT primary mirrors are recoated on 2-year cycle and washed in between years, but, as our campaign started during the pandemic, this recoating schedule was interrupted. The adaptive secondary (AdSec) mirrors were generally used, but occasional technical downtime of one or other AdSec mirror required the observatory to swap in a rigid secondary mirror which has a slightly different aluminum coating. Various jumps in throughput seen are all aligned with observatory

¹⁶ <https://archive.lbto.org/>

¹⁷ A description of the modIDL pipeline can be found in D. A. Berg et al. (2015).

records of when the primary mirrors were washed or recoated and times when the rigid secondary was swapped in and out.

The primary difference between MODS1 and MODS2 throughput during our campaign was that the aluminum coating on the adaptive secondary mirror on the left-side of the LBT, where MODS1 is mounted, had been steadily degrading for many years. The net effect of this degradation was an overall loss of throughput on the left side of LBT for all instruments of ~ 0.5 – 0.6 magnitudes. When the left adaptive secondary was recoated in summer 2023, the MODS1 throughput returned to near-historical values, but still ~ 0.1 mag lower than the original MODS1 commissioning throughput due to the steady accumulation of dust on the internal spectrograph optics over 13 years of operation. MODS2, mounted on the right side of LBT, showed slow monotonic decline mostly due to the primary mirrors and some slow accumulation of dust on the internal optics, but a discontinuous change occurred after the recoating of the right-hand mirror in summer 2023, and the aluminum coating manifested a "blue haze" that degraded the throughput at blue wavelengths. We see this as a slight change in the slope of the MODS2 blue channel response functions before and after recoating.

Overall, our retrospective analysis of MODS calibration star data spanning our campaign shows that the basic shape of the spectral response functions was as stable as can be expected for optical coatings exposed to the environment. This allowed us to select a subset of the best calibration data from the entire span of the observing campaign for our calibrations. The calibrations for our sample are very well understood, something that is not possible for data sets collected from many disparate telescopes and instruments with no control over the calibration procedure or ability to perform a quantitative re-analysis of the calibration process.

Using the best calibration stars, we fit the response functions and, comparing with the cataloged primary flux calibrator data (R. C. Bohlin et al. 2019), we compute estimates of the random errors in the spectrophotometry contributed by the relative spectral response calibration. The resulting error functions are shown in Figure 2. The MODS blue channel relative flux calibration is typically good to $\pm 0.5\%$, with the expected increase in error to ± 1 – 2% at the extreme wavelength ends of the spectrum due to the combined fall-off in CCD detector quantum efficiency, grating blaze efficiency, and dichroic beam splitter transmission at the extreme blue/near-UV end of the spectrum, and into the dichroic cross-over at the red end. The MODS red channel relative flux calibration is typically $\pm 0.6\%$ over most of the range, with the expected increase at the blue end from the dichroic cross-over, and the monotonic decline in CCD detector quantum efficiency and grating blaze efficiency at the red end. Unlike the blue channel, the red channel also has im-

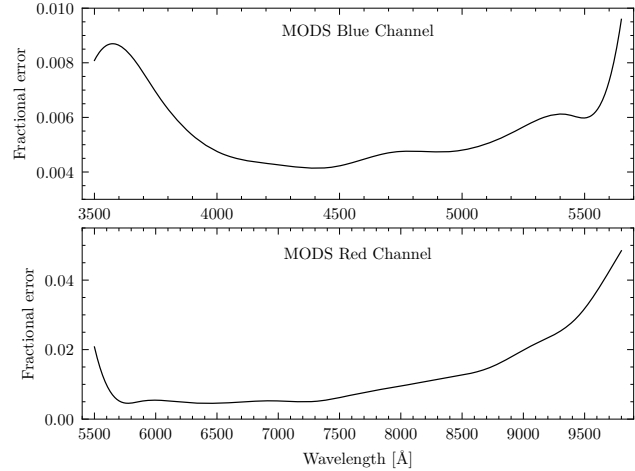


Figure 2. Spectral flux calibration error functions for the MODS blue and red grating spectrograph channels derived from archival and new observations of HST primary flux calibration stars. Curves show the fractional error in relative flux as a function of wavelength.

pacts due to telluric absorption starting at wavelengths longward of 6800\AA , which are difficult to correct for, leaving gaps in the response function that we interpolate across. The interpolations are informed by a subset of standard stars for which we have been able to compute reasonable model telluric corrections for data taken at low airmass on nights with a low precipitable water-vapor (PWV) column density (at the time LBTO site weather telemetry did not provide consistent contemporaneous PWV measurements with the radiometer at the Hertz mm-wave telescope on the summit of Mt. Graham). The fidelity of these interpolations is high as changes in actual instrumental response are expected to be very smooth on smaller scales (due to the physics of CCDs and the stability of the optical coatings).

Details of the MODS data reduction and presentation and analysis of the final 1D optical spectra will be given in Paper II.

3.2. Near-Infrared Spectroscopy

3.2.1. Observing Strategy

Because the $\text{He I} \lambda 10830\text{\AA}$ emission line provides a strong constraint on the nebular density and breaks the temperature-density degeneracy, we have used the LBT's LUCI (LBT Utility Camera in the Infrared) spectrographs (W. Seifert et al. 2003) to obtain a near-IR spectrum for most of the sample. For a minority of the targets (11 targets), we have adopted values from the literature. Over the course of the program, both LUCI instruments were not always available, so some observations come from a single LUCI spectrograph, and some have observations from both instruments.

LUCI long-slit spectra were taken with the G200 grating ($200 \text{ lines mm}^{-1}$) in second order with the zJ-band order-

separation filter to obtain a spectral resolution of ~ 2100 in the 0.9 to $1.35\mu\text{m}$ wavelength region that includes the $\text{He I } \lambda 10830\text{\AA}$ and $\text{H I } \text{P}\gamma$ emission lines over the range of redshifts of our targets. We used the facility 1-arcsec wide long-slit mask (LS-1.00arcsec), which is 205-arcsec long, providing simultaneous measurement of the galaxy and surrounding night sky. This is the same slit width used for the MODS visible-light spectra. When LUCI1 and LUCI2 were both available they were configured identically. Observations were taken when visible-light seeing was $<1.^{\prime\prime}1$, although on a few occasions we obtained acceptable observations in variable seeing. LUCI spectra were prioritized by the outcome of earlier MODS observing during our blocks of runs, but we never observed with both instruments on the same night. In total, we obtained high-quality LUCI near-IR spectra of 48 targets new for a total of 72 hours (wall clock time) of LBT time. We include our archival LUCI spectra of Leo P (E. Aver et al. 2021) in our analysis for a total of 49 LUCI observations.

Each target was observed for 1-hour total integration time acquired as a sequence of six (6) 600-second integrations in which we offset between two positions separated by $10''$ along the slit in an ABBAAB dither pattern. In a small number of galaxies, nearby structures along the slit required us to use a $20''$ dither spacing. This dither pattern allows for very clean sky subtraction in a spectral region which is crowded with many bright telluric OH airglow emission lines. All targets were observed at low airmass, and in this spectral range differential atmospheric refraction is negligible, unlike the case with MODS.

The wavelength calibration was determined using terrestrial OH airglow emission lines that appear in the longslit spectra with the wavelengths tabulated by P. Rousselot et al. (2000), and we used quartz lamp spectral flats and darks obtained on or close to the nights of LUCI observation. Like the MODS, the LUCIs are mounted on the telescope full-time except for summer shutdowns, and historically have had very stable internal detector calibrations. Bad pixel maps for the LUCIs' H2RG HgCdTe arrays are historically very stable, our targets are faint enough that we did not have problems with persistent image on the sensors, and we were careful when observing tellurics before science targets to not saturate the arrays.

3.2.2. Spectral Calibration

Spectral calibration for near-IR observing requires a different approach than the optical, relying traditionally on observations of A0V and A1V spectral type telluric stars selected using the Gemini Observatory Telluric Standard

Search tool¹⁸. We selected telluric stars matched to each target such that they would be observed at the same airmass as the target either before or after the science observations. The telluric star spectra provide a correction for atmospheric absorption in the zJ band, and a baseline relative flux calibration around the He I line. However, unlike with the MODS, the standard practice with the LUCIs is to not do a detailed end-to-end response calibration. Instead, we rely on the fact the relative fluxes of lines of interest are closely spaced and the measured spectral response functions for LUCI are very well behaved on such small wavelength scales. However, we made observations of the same HST primary calibrators we used with MODS on two observing runs and verified our assumptions are correct.

Details of the LUCI data reduction and presentation and analysis of the final 1D near-IR spectra will be given in Paper III.

4. NEW H AND HE EMISSIVITIES

4.1. H emissivities

Our previous work used the “Case B” H emissivities presented in D. G. Hummer & P. J. Storey (1987). These had been updated by P. J. Storey & T. Sochi (2015). T. Hsyu et al. (2020) reported a new set of H emissivities from P. Storey (2018, private communication). These emissivities extend the P. J. Storey & T. Sochi (2015) hydrogen emissivities down to $\log_{10}(n_e/\text{cm}^{-3})=0$, and are calculated on a fine grid up to $\log_{10}(n_e/\text{cm}^{-3})=5$ at $\log_{10}(n_e/\text{cm}^{-3})=1$ intervals. The grid used by T. Hsyu et al. (2020) stopped at the $n=10$ level, and was therefore not suitable for our purpose. P. Storey (2023, private communication) provided us with an even finer grid extended to the $n=15$ level.

We use bilinear interpolation within this temperature and density grid. We assume no error in the emissivity value as this is difficult to quantify, and we assume that the uncertainties on the H emissivities are sub-dominant to the other uncertainties in our procedure. This assumption is supported by the work of T. Hsyu et al. (2020) who compared the new $\text{H}\beta$ emissivity with that of R. L. Porter, as presented in E. Aver et al. (2010). They found differences in the range of 0.10 to 0.55%. T. Hsyu et al. (2020) also compared the new P. J. Storey & T. Sochi (2015) emissivities for the three strongest Balmer line ratios to the E. Aver et al. (2010) fit (based upon D. G. Hummer & P. J. Storey 1987) and found differences in the range from 0.10 to 0.20%. These very small differences between the most recent calculations support our assumption that the uncertainties on the H emissivities are neg-

¹⁸ <https://www.gemini.edu/observing/resources/near-ir-resources/spectroscopy/telluric-standard-search>

ligible. The details of these new H emissivities are discussed in Paper IV.

4.2. *He Emissivities*

Our previous work used the “Case B” He emissivities from R. L. Porter et al. (2012, 2013) calculated on a finer grid, as reported in E. Aver et al. (2013). Motivated by their discovery that the He recombination spectrum could be significantly improved (G. Del Zanna et al. 2020), G. Del Zanna & P. J. Storey (2022) have produced new He emissivities, and, unlike the case for H, found differences in excess of 1% when compared to previous studies. They provide a comprehensive overview of and comparison with previous studies. The biggest change relevant for our purpose is found in the $\lambda 6678$ line, which shows good agreement at low temperatures, but increasing discrepancies as the density and temperature increase. We adopt these new He emissivities, and, although the case is not as secure as for the H emissivities, we assume no uncertainties in the He emissivities, given the lack of quantified estimates. The details of these new He emissivities are discussed in Paper IV.

5. LBT Y_p PROJECT 1D SPECTRAL DATABASE

Because of their potential interest to the wider community, the publication of the primary results of this project will be accompanied by release of our 1D spectral data products in the form of machine-readable tables of our measured spectral lines fluxes in optical and infrared, and machine-readable ASCII tables of the extracted, wavelength- and flux-calibrated 1D spectra.

The near-infrared 1D spectral database will consist of the measured spectral line fluxes and 1D calibration spectra will be released as part of Paper III. The 1D merged LUCI spectra will be 3-column ASCII tables with wavelengths, relative fluxes, and flux errors.

The optical 1D spectral database will be released in two parts. The tables of hydrogen and helium emission line fluxes and uncertainties and derived nebular properties (O/H, temperature, density, etc.) used in the analysis in Paper IV will be released as part of Paper II. The full measured spectral line database (all species, not just the H and He lines), and the 1D wavelength- and flux calibrated MODS spectra will be released as part of Paper VI. The format of the 1D merged MODS spectra will be in the same 3-column ASCII format as the LUCI near-infrared spectra.

6. SUMMARY

6.1. *Overall Project Goal*

A simple back of the envelope calculation tells us that the helium mass fraction is $\sim 25\%$ from SBBN. That the helium abundance is observed to be around 25% played a big role in supporting the big bang theory over competing cosmological theories, as stars alone are not capable of producing the

requisite helium abundance. However, to fully test big bang cosmology and Standard Model physics, high-precision data are needed. Historically the helium abundance in big bang nucleosynthesis depends on three quantities: the baryon density, the neutron mean-life, and the number of relativistic species present at the time of nucleosynthesis (K. A. Olive et al. 1981). The latter can be characterized by the number of neutrino flavors. Precision on the baryon density is achieved from CMB measurements of the anisotropy spectrum (first by WMAP (E. Komatsu et al. 2014) and later by *Planck* (Planck Collaboration et al. 2020)). The neutron mean-life is also known to high precision ($\sim 0.05\%$) though there is currently a tension between different methods of determining the neutron lifetime. Its impact on BBN was recently reviewed in T.-H. Yeh et al. (2023). In the Standard Model, $N_\nu = 3$, and measured as $N_\nu = 2.9963 \pm 0.0074$ from the width of the Z gauge boson (P. Janot & S. Jadach 2020). This leads to the SBBN prediction $Y_p = 0.2467 \pm 0.0002$ (T.-H. Yeh et al. 2022, 2023), with better than 0.1% accuracy. Ultimately, we would like a comparable observational uncertainty to fully test the theory. In comparison, the current accuracy of the measured deuterium abundance is about 1%, though the theoretical uncertainty is much larger in this case.

Decades ago, helium abundance determinations were based on averaging the independently inferred abundances from three helium emission lines. The quoted uncertainties were typically of order 1%. These however ignored a whole host of systematic uncertainties. K. A. Olive & E. D. Skillman (2001, 2004) showed that there exist severe degeneracies in assumed physical parameters that, until resolved, would not permit a helium abundance determination to better than $\sim 5\%$. With a more rigorous approach to extracting a helium abundance, it was possible to obtain an uncertainty as low as $\sim 1.3\%$ (E. Aver et al. 2022). This determination still relied on a regression of the data with respect to metallicity with the primordial value resulting from the intercept of that regression. This procedure itself carries its own uncertainties, as we can not be sure that helium and oxygen track each other linearly. After all, there are different processes in different stars which produce these two elements.

Our goal in this series of papers is to produce an XMP sample of galaxies with high emission line fluxes. With a sufficiently large sample size of XMP galaxies, we could avoid relying on a regression (or assumed functional dependence) between helium and oxygen. We believe that we have made an important step towards this goal as detailed in this series of papers.

6.2. *Improvements to Our Methodology*

Our LBT Y_p Project methodology is built on the analyses reported in E. Aver et al. (2015, 2021, 2022). As described here, we have identified required characteristics of candidate

targets (low O/H, high H β flux, high H β equivalent width) in order to produce high-quality, useful measurements. We have optimized data reduction and analyses processes to produce high fidelity measurements with reliable uncertainties. We use the most modern H and He emissivities calculated on very fine grids. We use the most modern radiative transfer corrections following [O. Kurichin & A. Ivanchik \(2025\)](#). Other more subtle improvements in the analysis are described in Paper IV. In summary, in addition to gathering the desired high quality LBT observations, we have sought to improve every step of the data reduction and analysis chain.

6.3. Papers in this Series

In Paper II ([N. Rogers et al. 2026](#)), we describe the reduction of the LBT/MODS optical observations. This includes a new treatment of the emission line profiles in MODS, allowing for better constraints on emission line fluxes of blended features such as He I $\lambda 3889$ and H8. The optical line fluxes are used to derive the physical conditions of the gas and measure the total O/H abundance. The direct T_e [O III] in the interstellar medium is used as a weak prior on T_e (He I) in the MCMC analysis, but also provides an opportunity to examine scaling relations between T_e from other ions (e.g., S $^{2+}$ and O $^+$). The O/H abundances, which are traditionally required for the extrapolation of $\Delta Y/\Delta O$, have typical uncertainties of just 4%.

In Paper III ([M. Weller et al. 2026](#)), we describe the reduction of the LBT/LUCI observations. These observations include the critical He I $\lambda 10830$ line, which provides very strong constraints on the density. Improvements and optimizations upon the standard LUCI reduction pipeline are described, enabling robust, high quality measurements of the near-IR emission lines.

Paper IV ([E. Aver et al. 2026](#)) presents the derivations of the helium abundances of the individual objects, the screening of the sample for reliability, and the subsequent derivation of a new value of Y_p . The entire sample consists of 41 objects all with $O/H \leq 14.5 \times 10^{-5}$, and 15 of these objects have metallicities of $O/H \leq 4 \times 10^{-5}$. This low-metallicity sample of 15 objects is in the regime where evolutionary effects are minimal, allowing a derivation of Y_p from the weighted mean, free from the assumption of a linear relationship between Y and O/H. Full details of the analysis of the entire data set are provided in Paper IV.

Implications of the new result for Y_p are presented in Paper V ([T.-H. Yeh et al. 2026](#)). In particular, the new value of Y_p and its uncertainty are used to determine the energy density in radiation at the time of BBN. This is then used to constrain the number of relativistic degrees of freedom present at that time. This result is presented as a limit on the number of neutrino flavors and can be adapted to constrain a variety of

physics models extending beyond the Standard Model ([R. H. Cyburt et al. 2005](#); [T.-H. Yeh et al. 2022](#)).

The spectral database assembled as part of the LBT Y_p Project can be tapped for other science cases. In Paper VI ([N. Rogers et al., in prep](#)), we explore the chemical abundances of nine elements in the metal-poor interstellar medium. This represents one of the largest homogeneous databases of high-quality multi-element abundances in low-Z nebulae, which is required to interpret emerging abundance trends at high- z acquired with JWST.

ACKNOWLEDGEMENTS

This work was supported by funds provided by NSF Collaborative Research Grants AST-2205817 to RWP, AST-2205864 to EDS, and AST-2205958 to EA. Our team workshop at OSU in July 2024 was sponsored in part by OSU’s Center for Cosmology and AstroParticle Physics (CCAPP). The work of KAO was supported in part by DOE grant DE-SC0011842 at the University of Minnesota. TRIUMF receives federal funding via a contribution agreement with the National Research Council of Canada.

This work is based on observations made with the Large Binocular Telescope. The LBT is an international collaboration among institutions in the United States, Italy and Germany. LBT Corporation Members are: The University of Arizona on behalf of the Arizona Board of Regents; Istituto Nazionale di Astrofisica, Italy; LBT Beteiligungsellschaft, Germany, representing the Max-Planck Society, The Leibniz Institute for Astrophysics Potsdam, and Heidelberg University; The Ohio State University, and The Research Corporation, on behalf of The University of Notre Dame, University of Minnesota and University of Virginia. Observations have benefited from the use of ALTA Center ([alta.arcetri.inaf.it](#)) forecasts performed with the Astro-Meso-Nh model. Initialization data of the ALTA automatic forecast system come from the General Circulation Model (HRES) of the European Centre for Medium Range Weather Forecasts.

This research used the facilities of the Italian Center for Astronomical Archive (IA2) operated by INAF at the Astronomical Observatory of Trieste.

All LBT observations for this project were executed remotely, beginning during the global COVID-19 pandemic when we all learned together how to operate the LBT from basements, spare bedrooms, and home offices. We are most grateful for the tireless efforts of the Mount Graham and Tucson technical and observing support staff of the Large Binocular Telescope Observatory who were critical to making it all work smoothly, keeping telescopes and instruments operating in top form under trying circumstances. The 130 hours

of high-quality, consistent spectrophotometric data acquired for this project would not have been possible without them.

EDS, KAO, EA, DAB, NSJR, and JHM would like to acknowledge and thank Stanley Hubbard for his generous gift

to the University of Minnesota that allowed the University to become a member of the LBT collaboration.

APPENDIX

A. METHODOLOGICAL DIFFERENCES BETWEEN AVER ET AL. (2015) AND HSYU ET AL. (2020)

[T. Hsyu et al. \(2020\)](#) independently coded the methodology of [E. Aver et al. \(2015\)](#) for their analysis. However, beyond any small differences in atomic data or number of emission lines used, there are some subtle but potentially important differences in the methodology. Specifically, [E. Aver et al. \(2015\)](#) use a χ^2 minimization to determine the best-fit (maximum likelihood) values for the model parameters and then follow with an MCMC analysis to determine the uncertainties on those values. The MCMC analysis is critical because it reveals degeneracies between various parameters ([E. Aver et al. 2011](#)). While [T. Hsyu et al. \(2020\)](#) follow the [E. Aver et al. \(2015\)](#) MCMC, they adopt final values for the parameters from the median values of the MCMC distribution. In typical cases, the minimization best fits and the median values from the MCMC analyses will be quite similar. However, in the cases where parameters are restricted to positive values (e.g., density, underlying stellar absorption, optical depth), and when the maximum likelihood values are small, the distribution of Markov Chain values will be truncated to positive values, with an asymmetric tail extending to higher values. This results in a median value significantly higher than the best-fit, maximum likelihood value. Furthermore, in the cases of parameters with maximum likelihood values approaching the zero lower bound, using the median value results in a lower limit for the parameter's uncertainty range that does not even encompass the maximum likelihood value. The impact of this bias is difficult to predict, but there will be departures from the best-fit values.

A second difference is in how objects “qualify” for inclusion in the determination of Y_p . [E. Aver et al. \(2012\)](#) introduced (within He abundance analyses) the concept of using the minimized χ^2 value (i.e., the best model fit to the observations) as a criterion for objects to qualify for use in the determination of Y_p . This provides a very direct and statistically rigorous way to assess the reliability of the results. [T. Hsyu et al. \(2020\)](#) use a different criterion. In order for objects to qualify in their analysis, they require that the measured and model-predicted values for all of their emission lines agree to within two σ (their Sample 1) or all but one line agree to within two σ (their Sample 2). Clearly, if their median parameter values are near their maximum likelihood values (as would be hoped), these both represent a lower threshold and allow a larger number of objects to be used in their Y_p analysis. It is not clear what the impact of this choice is on the value of Y_p , but it is likely that the uncertainty is reduced by including more objects in the analysis that likely would not have qualified using a χ^2 criterion.

A third important difference is the inhomogeneity of the observations in their sample. The importance of observing the He I $\lambda 10830$ emission line has been emphasized and they obtain He I $\lambda 10830$ observations for the 3 galaxies from their PHLEK sample and the 13 galaxies from the HeBCD sample have existing 10830 observations; however, they do not have He I $\lambda 10830$ observations for the 38 galaxies in their SDSS sample, the majority of the 54 systems in their Sample 1. We are not sure what the potential systematic effects are of not limiting the sample to systems with He I $\lambda 10830$ observations, beyond larger per object uncertainties on the derived He/H abundances

[A. Matsumoto et al. \(2022\)](#) and [H. Yanagisawa et al. \(2025\)](#) adopt the [T. Hsyu et al. \(2020\)](#) methodology, so the same differences as detailed above apply, with one revision. Motivated by the concerns above, [A. Matsumoto et al. \(2022\)](#) allows for unphysical, negative parameter values when analyzing the Subaru observations in their sample (though not for the literature values they take from [T. Hsyu et al. 2020](#)). Our approach is to retain the positive restriction, but use the maximum likelihood value, rather than the median value. Please see Section 1.2.2 for further details on the samples, analysis, and results in [A. Matsumoto et al. \(2022\)](#) and [H. Yanagisawa et al. \(2025\)](#).

Facilities: LBT (MODS), LBT (LUCI)

Software: astropy ([Astropy Collaboration et al. 2013, 2018, 2022](#)), jupyter ([T. Kluyver et al. 2016](#)), modsIDL ([K. V. Croxall & R. W. Pogge 2019](#)), modsCCDRed ([R. Pogge 2019](#)), PypeIt ([J. X. Prochaska et al. 2020; J. X. Prochaska et al. 2020](#)), PyNeb ([V. Luridiana et al. 2012, 2015](#)), numpy ([C. R. Harris et al. 2020](#)), matplotlib ([J. D. Hunter 2007](#))

REFERENCES

Abazajian, K., Addison, G., Adshead, P., et al. 2019, arXiv e-prints, arXiv:1907.04473, doi: [10.48550/arXiv.1907.04473](https://doi.org/10.48550/arXiv.1907.04473)

Addison, G. E., Watts, D. J., Bennett, C. L., et al. 2018, *ApJ*, 853, 119, doi: [10.3847/1538-4357/aaa1ed](https://doi.org/10.3847/1538-4357/aaa1ed)

Alonso-Álvarez, G., & Cline, J. M. 2022, *Phys. Lett. B*, 833, 137278, doi: [10.1016/j.physletb.2022.137278](https://doi.org/10.1016/j.physletb.2022.137278)

Arellano-Córdova, K. Z., & Rodríguez, M. 2020, *MNRAS*, 497, 672, doi: [10.1093/mnras/staa1759](https://doi.org/10.1093/mnras/staa1759)

Astropy Collaboration, Robitaille, T. P., Tollerud, E. J., et al. 2013, *A&A*, 558, A33, doi: [10.1051/0004-6361/201322068](https://doi.org/10.1051/0004-6361/201322068)

Astropy Collaboration, Price-Whelan, A. M., Sipőcz, B. M., et al. 2018, *AJ*, 156, 123, doi: [10.3847/1538-3881/aabc4f](https://doi.org/10.3847/1538-3881/aabc4f)

Astropy Collaboration, Price-Whelan, A. M., Lim, P. L., et al. 2022, *ApJ*, 935, 167, doi: [10.3847/1538-4357/ac7c74](https://doi.org/10.3847/1538-4357/ac7c74)

Aver, E., Berg, D. A., Hirschauer, A. S., et al. 2022, *MNRAS*, 510, 373, doi: [10.1093/mnras/stab3226](https://doi.org/10.1093/mnras/stab3226)

Aver, E., Berg, D. A., Olive, K. A., et al. 2021, *JCAP*, 2021, 027, doi: [10.1088/1475-7516/2021/03/027](https://doi.org/10.1088/1475-7516/2021/03/027)

Aver, E., Olive, K. A., Porter, R. L., & Skillman, E. D. 2013, *JCAP*, 2013, 017, doi: [10.1088/1475-7516/2013/11/017](https://doi.org/10.1088/1475-7516/2013/11/017)

Aver, E., Olive, K. A., & Skillman, E. D. 2010, *JCAP*, 2010, 003, doi: [10.1088/1475-7516/2010/05/003](https://doi.org/10.1088/1475-7516/2010/05/003)

Aver, E., Olive, K. A., & Skillman, E. D. 2011, *JCAP*, 2011, 043, doi: [10.1088/1475-7516/2011/03/043](https://doi.org/10.1088/1475-7516/2011/03/043)

Aver, E., Olive, K. A., & Skillman, E. D. 2012, *JCAP*, 2012, 004, doi: [10.1088/1475-7516/2012/04/004](https://doi.org/10.1088/1475-7516/2012/04/004)

Aver, E., Olive, K. A., & Skillman, E. D. 2015, *JCAP*, 2015, 011, doi: [10.1088/1475-7516/2015/07/011](https://doi.org/10.1088/1475-7516/2015/07/011)

Aver, E., et al. 2026,

Balashev, S. A., Zavarygin, E. O., Ivanchik, A. V., Telikova, K. N., & Varshalovich, D. A. 2016, *MNRAS*, 458, 2188, doi: [10.1093/mnras/stw356](https://doi.org/10.1093/mnras/stw356)

Barger, V., Langacker, P., & Lee, H.-S. 2003, *Phys. Rev. D*, 67, 075009, doi: [10.1103/PhysRevD.67.075009](https://doi.org/10.1103/PhysRevD.67.075009)

Benjamin, R. A., Skillman, E. D., & Smits, D. P. 2002, *ApJ*, 569, 288, doi: [10.1086/339242](https://doi.org/10.1086/339242)

Berg, D. A., Skillman, E. D., Croxall, K. V., et al. 2015, *ApJ*, 806, 16, doi: [10.1088/0004-637X/806/1/16](https://doi.org/10.1088/0004-637X/806/1/16)

Bohlin, R. C., Deustua, S. E., & de Rosa, G. 2019, *AJ*, 158, 211, doi: [10.3847/1538-3881/ab480c](https://doi.org/10.3847/1538-3881/ab480c)

Bohlin, R. C., Gordon, K. D., & Tremblay, P. E. 2014, *PASP*, 126, 711, doi: [10.1086/677655](https://doi.org/10.1086/677655)

Böser, S., Buck, C., Giunti, C., et al. 2020, *Progress in Particle and Nuclear Physics*, 111, 103736, doi: [10.1016/j.ppnp.2019.103736](https://doi.org/10.1016/j.ppnp.2019.103736)

Boyle, L. A., & Buonanno, A. 2008, *Phys. Rev. D*, 78, 043531, doi: [10.1103/PhysRevD.78.043531](https://doi.org/10.1103/PhysRevD.78.043531)

Calabrese, E., et al. 2025, *JCAP*, 11, 063, doi: [10.1088/1475-7516/2025/11/063](https://doi.org/10.1088/1475-7516/2025/11/063)

Camphuis, E., et al. 2025, <https://arxiv.org/abs/2506.20707>

Cooke, R. J., & Fumagalli, M. 2018, *Nature Astronomy*, 2, 957, doi: [10.1038/s41550-018-0584-z](https://doi.org/10.1038/s41550-018-0584-z)

Cooke, R. J., Pettini, M., Jorgenson, R. A., Murphy, M. T., & Steidel, C. C. 2014, *ApJ*, 781, 31, doi: [10.1088/0004-637X/781/1/31](https://doi.org/10.1088/0004-637X/781/1/31)

Cooke, R. J., Pettini, M., Nollett, K. M., & Jorgenson, R. 2016, *ApJ*, 830, 148, doi: [10.3847/0004-637X/830/2/148](https://doi.org/10.3847/0004-637X/830/2/148)

Cooke, R. J., Pettini, M., & Steidel, C. C. 2018, *ApJ*, 855, 102, doi: [10.3847/1538-4357/aaab53](https://doi.org/10.3847/1538-4357/aaab53)

Croxall, K. V., & Pogge, R. W. 2019, *rwpogge/modsIDL*: modsIDL Binocular Release, v1.0 Zenodo, doi: [10.5281/zenodo.2561424](https://doi.org/10.5281/zenodo.2561424)

Cyburt, R. H., Fields, B. D., & Olive, K. A. 2002, *Astroparticle Physics*, 17, 87, doi: [10.1016/S0927-6505\(01\)00171-2](https://doi.org/10.1016/S0927-6505(01)00171-2)

Cyburt, R. H., Fields, B. D., & Olive, K. A. 2008, *JCAP*, 11, 012, doi: [10.1088/1475-7516/2008/11/012](https://doi.org/10.1088/1475-7516/2008/11/012)

Cyburt, R. H., Fields, B. D., Olive, K. A., & Skillman, E. 2005, *Astroparticle Physics*, 23, 313, doi: [10.1016/j.astropartphys.2005.01.005](https://doi.org/10.1016/j.astropartphys.2005.01.005)

Cyburt, R. H., Fields, B. D., Olive, K. A., & Yeh, T.-H. 2016, *Reviews of Modern Physics*, 88, 015004, doi: [10.1103/RevModPhys.88.015004](https://doi.org/10.1103/RevModPhys.88.015004)

Del Zanna, G., & Storey, P. J. 2022, *MNRAS*, 513, 1198, doi: [10.1093/mnras/stac800](https://doi.org/10.1093/mnras/stac800)

Del Zanna, G., Storey, P. J., Badnell, N. R., & Andretta, V. 2020, *ApJ*, 898, 72, doi: [10.3847/1538-4357/ab9d84](https://doi.org/10.3847/1538-4357/ab9d84)

Dolgov, A. D., & Villante, F. L. 2004, *Nucl. Phys. B*, 679, 261, doi: [10.1016/j.nuclphysb.2003.11.031](https://doi.org/10.1016/j.nuclphysb.2003.11.031)

Drewes, M., Georis, Y., Klasen, M., Wiggering, L. P., & Wong, Y. Y. 2024, *JCAP*, 06, 032, doi: [10.1088/1475-7516/2024/06/032](https://doi.org/10.1088/1475-7516/2024/06/032)

Eldridge, J. J., & Stanway, E. R. 2009, *MNRAS*, 400, 1019, doi: [10.1111/j.1365-2966.2009.15514.x](https://doi.org/10.1111/j.1365-2966.2009.15514.x)

Eldridge, J. J., Stanway, E. R., Xiao, L., et al. 2017, *PASA*, 34, e058, doi: [10.1017/pasa.2017.51](https://doi.org/10.1017/pasa.2017.51)

Ferland, G. J., Izotov, Y., Peimbert, A., et al. 2010, in IAU Symposium, Vol. 268, Light Elements in the Universe, ed. C. Charbonnel, M. Tosi, F. Primas, & C. Chiappini, 163–167, doi: [10.1017/S1743921310004011](https://doi.org/10.1017/S1743921310004011)

Fernández, V., Terlevich, E., Díaz, A. I., & Terlevich, R. 2019, *MNRAS*, 487, 3221, doi: [10.1093/mnras/stz1433](https://doi.org/10.1093/mnras/stz1433)

Fernández, V., Terlevich, E., Díaz, A. I., Terlevich, R., & Rosales-Ortega, F. F. 2018, *MNRAS*, 478, 5301, doi: [10.1093/mnras/sty1206](https://doi.org/10.1093/mnras/sty1206)

Fields, B. D., & Olive, K. A. 1998, *Astrophys. J.*, 506, 177, doi: [10.1086/306248](https://doi.org/10.1086/306248)

Fields, B. D., & Olive, K. A. 2022, *JCAP*, 10, 078, doi: [10.1088/1475-7516/2022/10/078](https://doi.org/10.1088/1475-7516/2022/10/078)

Fields, B. D., Olive, K. A., Yeh, T.-H., & Young, C. 2020, *JCAP*, 2020, 010, doi: [10.1088/1475-7516/2020/03/010](https://doi.org/10.1088/1475-7516/2020/03/010)

Filippenko, A. V. 1982, *PASP*, 94, 715, doi: [10.1086/131052](https://doi.org/10.1086/131052)

Gonzalez-Garcia, M. C., & Valle, J. W. F. 1990, Phys. Lett. B, 240, 163, doi: [10.1016/0370-2693\(90\)90426-7](https://doi.org/10.1016/0370-2693(90)90426-7)

Guarneri, F., Pasquini, L., D'Odorico, V., et al. 2024, Mon. Not. Roy. Astron. Soc., 529, 839, doi: [10.1093/mnras/stae452](https://doi.org/10.1093/mnras/stae452)

Guseva, N. G., Izotov, Y. I., Fricke, K. J., & Henkel, C. 2015, A&A, 579, A11, doi: [10.1051/0004-6361/201525697](https://doi.org/10.1051/0004-6361/201525697)

Guseva, N. G., Izotov, Y. I., Fricke, K. J., & Henkel, C. 2017, A&A, 599, A65, doi: [10.1051/0004-6361/201629181](https://doi.org/10.1051/0004-6361/201629181)

Harris, C. R., Millman, K. J., van der Walt, S. J., et al. 2020, Nature, 585, 357, doi: [10.1038/s41586-020-2649-2](https://doi.org/10.1038/s41586-020-2649-2)

Hill, J. M. 2010, ApOpt, 49, D115, doi: [10.1364/AO.49.00D115](https://doi.org/10.1364/AO.49.00D115)

Hirschauer, A. S., Salzer, J. J., Skillman, E. D., et al. 2016, ApJ, 822, 108, doi: [10.3847/0004-637X/822/2/108](https://doi.org/10.3847/0004-637X/822/2/108)

Hsyu, T., Cooke, R. J., Prochaska, J. X., & Bolte, M. 2017, ApJL, 845, L22, doi: [10.3847/2041-8213/aa821f](https://doi.org/10.3847/2041-8213/aa821f)

Hsyu, T., Cooke, R. J., Prochaska, J. X., & Bolte, M. 2018, ApJ, 863, 134, doi: [10.3847/1538-4357/aad18a](https://doi.org/10.3847/1538-4357/aad18a)

Hsyu, T., Cooke, R. J., Prochaska, J. X., & Bolte, M. 2020, ApJ, 896, 77, doi: [10.3847/1538-4357/ab91af](https://doi.org/10.3847/1538-4357/ab91af)

Hummer, D. G., & Storey, P. J. 1987, MNRAS, 224, 801, doi: [10.1093/mnras/224.3.801](https://doi.org/10.1093/mnras/224.3.801)

Hunter, J. D. 2007, Computing in Science and Engineering, 9, 90, doi: [10.1109/MCSE.2007.55](https://doi.org/10.1109/MCSE.2007.55)

Iocco, F., Mangano, G., Miele, G., Pisanti, O., & Serpico, P. D. 2009, Phys. Rept., 472, 1, doi: [10.1016/j.physrep.2009.02.002](https://doi.org/10.1016/j.physrep.2009.02.002)

Izotov, Y. I., Stasińska, G., & Guseva, N. G. 2013, A&A, 558, A57, doi: [10.1051/0004-6361/201220782](https://doi.org/10.1051/0004-6361/201220782)

Izotov, Y. I., Thuan, T. X., & Guseva, N. G. 2014, MNRAS, 445, 778, doi: [10.1093/mnras/stu1771](https://doi.org/10.1093/mnras/stu1771)

Izotov, Y. I., Thuan, T. X., & Guseva, N. G. 2019, MNRAS, 483, 5491, doi: [10.1093/mnras/sty3472](https://doi.org/10.1093/mnras/sty3472)

Izotov, Y. I., Thuan, T. X., Guseva, N. G., & Liss, S. E. 2018, MNRAS, 473, 1956, doi: [10.1093/mnras/stx2478](https://doi.org/10.1093/mnras/stx2478)

Izotov, Y. I., Thuan, T. X., & Stasińska, G. 2007, ApJ, 662, 15, doi: [10.1086/513601](https://doi.org/10.1086/513601)

Janot, P., & Jadach, S. 2020, Phys. Lett. B, 803, 135319, doi: [10.1016/j.physletb.2020.135319](https://doi.org/10.1016/j.physletb.2020.135319)

Jedamzik, K., & Pospelov, M. 2009, New J. Phys., 11, 105028, doi: [10.1088/1367-2630/11/10/105028](https://doi.org/10.1088/1367-2630/11/10/105028)

Kislitsyn, P. A., Balashev, S. A., Murphy, M. T., et al. 2024, Mon. Not. Roy. Astron. Soc., 528, 4068, doi: [10.1093/mnras/stae248](https://doi.org/10.1093/mnras/stae248)

Kluyver, T., Ragan-Kelley, B., Pérez, F., et al. 2016, in Positioning and Power in Academic Publishing: Players, Agents and Agendas, ed. F. Loizides & B. Schmidt, IOS Press, 87 – 90

Kohri, K., & Terada, T. 2018, PhRvD, 97, 123532, doi: [10.1103/PhysRevD.97.123532](https://doi.org/10.1103/PhysRevD.97.123532)

Kojima, T., Ouchi, M., Rauch, M., et al. 2020, ApJ, 898, 142, doi: [10.3847/1538-4357/aba047](https://doi.org/10.3847/1538-4357/aba047)

Kojima, T., Ouchi, M., Rauch, M., et al. 2021, ApJ, 913, 22, doi: [10.3847/1538-4357/abec3d](https://doi.org/10.3847/1538-4357/abec3d)

Komatsu, E., Bennett, C. L., Barnes, C., et al. 2014, Progress of Theoretical and Experimental Physics, 2014, 06B102, doi: [10.1093/ptep/ptu083](https://doi.org/10.1093/ptep/ptu083)

Kurichin, O., & Ivanchik, A. 2025, arXiv e-prints, arXiv:2510.02045, doi: [10.48550/arXiv.2510.02045](https://doi.org/10.48550/arXiv.2510.02045)

Kurichin, O. A., & Ivanchik, A. V. 2024, Astronomy Letters, 50, 807, doi: [10.1134/S1063773725700070](https://doi.org/10.1134/S1063773725700070)

Kurichin, O. A., Kislytsyn, P. A., & Ivanchik, A. V. 2021a, Astronomy Letters, 47, 674, doi: [10.1134/S1063773721100054](https://doi.org/10.1134/S1063773721100054)

Kurichin, O. A., Kislytsyn, P. A., Klimenko, V. V., Balashev, S. A., & Ivanchik, A. V. 2021b, MNRAS, 502, 3045, doi: [10.1093/mnras/stab215](https://doi.org/10.1093/mnras/stab215)

Luridiana, V., Morisset, C., & Shaw, R. A. 2012, IAU Symposium, 283, 422, doi: [10.1017/S1743921312011738](https://doi.org/10.1017/S1743921312011738)

Luridiana, V., Morisset, C., & Shaw, R. A. 2015, A&A, 573, A42, doi: [10.1051/0004-6361/201323152](https://doi.org/10.1051/0004-6361/201323152)

Luridiana, V., Peimbert, A., Peimbert, M., & Cerviño, M. 2003, ApJ, 592, 846, doi: [10.1086/375774](https://doi.org/10.1086/375774)

Matsumoto, A., Ouchi, M., Nakajima, K., et al. 2022, ApJ, 941, 167, doi: [10.3847/1538-4357/ac9ea1](https://doi.org/10.3847/1538-4357/ac9ea1)

McQuinn, K. B. W., Berg, D. A., Skillman, E. D., et al. 2020, ApJ, 891, 181, doi: [10.3847/1538-4357/ab7447](https://doi.org/10.3847/1538-4357/ab7447)

Navas, S., et al. 2024, Phys. Rev. D, 110, 030001, doi: [10.1103/PhysRevD.110.030001](https://doi.org/10.1103/PhysRevD.110.030001)

Oke, J. B. 1990, AJ, 99, 1621, doi: [10.1086/115444](https://doi.org/10.1086/115444)

Olive, K. A., Schramm, D. N., Steigman, G., Turner, M. S., & Yang, J.-M. 1981, Astrophys. J., 246, 557, doi: [10.1086/158956](https://doi.org/10.1086/158956)

Olive, K. A., & Skillman, E. D. 2001, NewA, 6, 119, doi: [10.1016/S1384-1076\(01\)00051-3](https://doi.org/10.1016/S1384-1076(01)00051-3)

Olive, K. A., & Skillman, E. D. 2004, ApJ, 617, 29, doi: [10.1086/425170](https://doi.org/10.1086/425170)

Olive, K. A., Steigman, G., & Walker, T. P. 2000, PhR, 333, 389, doi: [10.1016/S0370-1573\(00\)00031-4](https://doi.org/10.1016/S0370-1573(00)00031-4)

Peimbert, A., Peimbert, M., & Luridiana, V. 2016, RMxAA, 52, 419, doi: [10.48550/arXiv.1608.02062](https://doi.org/10.48550/arXiv.1608.02062)

Peimbert, M., Luridiana, V., & Peimbert, A. 2007, ApJ, 666, 636, doi: [10.1086/520571](https://doi.org/10.1086/520571)

Peimbert, M., & Torres-Peimbert, S. 1974, ApJ, 193, 327, doi: [10.1086/153166](https://doi.org/10.1086/153166)

Pilyugin, L. S. 1993, A&A, 277, 42

Pitrou, C., Coc, A., Uzan, J.-P., & Vangioni, E. 2018, Phys. Rept., 754, 1, doi: [10.1016/j.physrep.2018.04.005](https://doi.org/10.1016/j.physrep.2018.04.005)

Planck Collaboration, Aghanim, N., Akrami, Y., et al. 2020, A&A, 641, A6, doi: [10.1051/0004-6361/201833910](https://doi.org/10.1051/0004-6361/201833910)

Pogge, R. 2019, rwpogge/modsCCDRed: v2.0.1, 2.0.1 Zenodo, doi: [10.5281/zenodo.2647501](https://doi.org/10.5281/zenodo.2647501)

Pogge, R. W., Atwood, B., Brewer, D. F., et al. 2010, in Society of Photo-Optical Instrumentation Engineers (SPIE) Conference Series, Vol. 7735, Ground-based and Airborne Instrumentation for Astronomy III, ed. I. S. McLean, S. K. Ramsay, & H. Takami, 77350A, doi: [10.1117/12.857215](https://doi.org/10.1117/12.857215)

Porter, R. L., Ferland, G. J., Storey, P. J., & Detisch, M. J. 2012, MNRAS, 425, L28, doi: [10.1111/j.1745-3933.2012.01300.x](https://doi.org/10.1111/j.1745-3933.2012.01300.x)

Porter, R. L., Ferland, G. J., Storey, P. J., & Detisch, M. J. 2013, MNRAS, 433, L89, doi: [10.1093/mnrasl/slt049](https://doi.org/10.1093/mnrasl/slt049)

Pospelov, M., & Pradler, J. 2010, Ann. Rev. Nucl. Part. Sci., 60, 539, doi: [10.1146/annurev.nucl.012809.104521](https://doi.org/10.1146/annurev.nucl.012809.104521)

Prochaska, J. X., Hennawi, J. F., Westfall, K. B., et al. 2020, Journal of Open Source Software, 5, 2308, doi: [10.21105/joss.02308](https://doi.org/10.21105/joss.02308)

Prochaska, J. X., Hennawi, J., Cooke, R., et al. 2020, pypeit/PyPeIt: Release 1.0.0, v1.0.0 Zenodo, doi: [10.5281/zenodo.3743493](https://doi.org/10.5281/zenodo.3743493)

Pustilnik, S. A., Egorova, E. S., Kniazev, A. Y., et al. 2021, MNRAS, 507, 944, doi: [10.1093/mnras/stab2084](https://doi.org/10.1093/mnras/stab2084)

Pustilnik, S. A., Kniazev, A. Y., Perepelitsyna, Y. A., & Egorova, E. S. 2020, MNRAS, 493, 830, doi: [10.1093/mnras/staa215](https://doi.org/10.1093/mnras/staa215)

Riener-Sørensen, S., Kotuš, S., Webb, J. K., et al. 2017, MNRAS, 468, 3239, doi: [10.1093/mnras/stx681](https://doi.org/10.1093/mnras/stx681)

Riener-Sørensen, S., Webb, J. K., Crighton, N., et al. 2015, MNRAS, 447, 2925, doi: [10.1093/mnras/stu2599](https://doi.org/10.1093/mnras/stu2599)

Riess, A. G., Casertano, S., Yuan, W., et al. 2021, ApJL, 908, L6, doi: [10.3847/2041-8213/abdbaf](https://doi.org/10.3847/2041-8213/abdbaf)

Riess, A. G., Casertano, S., Yuan, W., Macri, L. M., & Scolnic, D. 2019, ApJ, 876, 85, doi: [10.3847/1538-4357/ab1422](https://doi.org/10.3847/1538-4357/ab1422)

Rogers, N., et al. 2026,

Rogers, N. S. J., Skillman, E. D., Pogge, R. W., et al. 2022, ApJ, 939, 44, doi: [10.3847/1538-4357/ac947d](https://doi.org/10.3847/1538-4357/ac947d)

Rogers, N. S. J., Skillman, E. D., Pogge, R. W., et al. 2021, ApJ, 915, 21, doi: [10.3847/1538-4357/abf8b9](https://doi.org/10.3847/1538-4357/abf8b9)

Rousselot, P., Lidman, C., Cuby, J. G., Moreels, G., & Monnet, G. 2000, A&A, 354, 1134

Sabti, N., Alvey, J., Escudero, M., Fairbairn, M., & Blas, D. 2020, JCAP, 2020, 004, doi: [10.1088/1475-7516/2020/01/004](https://doi.org/10.1088/1475-7516/2020/01/004)

Sánchez Almeida, J., Filho, M. E., Dalla Vecchia, C., & Skillman, E. D. 2017, ApJ, 835, 159, doi: [10.3847/1538-4357/835/2/159](https://doi.org/10.3847/1538-4357/835/2/159)

Sarkar, S. 1996, Rept. Prog. Phys., 59, 1493, doi: [10.1088/0034-4885/59/12/001](https://doi.org/10.1088/0034-4885/59/12/001)

Scholte, D., Cullen, F., Moustakas, J. M., et al. 2026, arXiv e-prints, arXiv:2601.02463, doi: [10.48550/arXiv.2601.02463](https://doi.org/10.48550/arXiv.2601.02463)

Schöneberg, N., Lesgourgues, J., & Hooper, D. C. 2019, JCAP, 2019, 029, doi: [10.1088/1475-7516/2019/10/029](https://doi.org/10.1088/1475-7516/2019/10/029)

Seifert, W., Appenzeller, I., Baumeister, H., et al. 2003, in Society of Photo-Optical Instrumentation Engineers (SPIE) Conference Series, Vol. 4841, Instrument Design and Performance for Optical/Infrared Ground-based Telescopes, ed. M. Iye & A. F. M. Moorwood, 962–973, doi: [10.1117/12.459494](https://doi.org/10.1117/12.459494)

Senchyna, P., & Stark, D. P. 2019, MNRAS, 484, 1270, doi: [10.1093/mnras/stz058](https://doi.org/10.1093/mnras/stz058)

Stanway, E. R., & Eldridge, J. J. 2018, MNRAS, 479, 75, doi: [10.1093/mnras/sty1353](https://doi.org/10.1093/mnras/sty1353)

Steigman, G., Olive, K. A., Schramm, D. N., & Turner, M. S. 1986, Phys. Lett. B, 176, 33, doi: [10.1016/0370-2693\(86\)90920-2](https://doi.org/10.1016/0370-2693(86)90920-2)

Steigman, G., Schramm, D. N., & Gunn, J. E. 1977, Phys. Lett. B, 66, 202, doi: [10.1016/0370-2693\(77\)90176-9](https://doi.org/10.1016/0370-2693(77)90176-9)

Storey, P. J., & Sochi, T. 2015, MNRAS, 446, 1864, doi: [10.1093/mnras/stu2243](https://doi.org/10.1093/mnras/stu2243)

Valerdi, M., Peimbert, A., Peimbert, M., & Sixtos, A. 2019, ApJ, 876, 98, doi: [10.3847/1538-4357/ab14e4](https://doi.org/10.3847/1538-4357/ab14e4)

Weller, M., et al. 2026,

Yanagisawa, H., Ouchi, M., Matsumoto, A., et al. 2025, arXiv e-prints, arXiv:2506.24050, doi: [10.48550/arXiv.2506.24050](https://doi.org/10.48550/arXiv.2506.24050)

Yang, H., Malhotra, S., Rhoads, J. E., & Wang, J. 2017, ApJ, 847, 38, doi: [10.3847/1538-4357/aa8809](https://doi.org/10.3847/1538-4357/aa8809)

Yeh, T.-H., Olive, K. A., & Fields, B. D. 2023, Universe, 9, 183, doi: [10.3390/universe9040183](https://doi.org/10.3390/universe9040183)

Yeh, T.-H., Olive, K. A., & Fields, B. D. 2024, JCAP, 07, 016, doi: [10.1088/1475-7516/2024/07/016](https://doi.org/10.1088/1475-7516/2024/07/016)

Yeh, T.-H., Shelton, J., Olive, K. A., & Fields, B. D. 2022, JCAP, 10, 046, doi: [10.1088/1475-7516/2022/10/046](https://doi.org/10.1088/1475-7516/2022/10/046)

Yeh, T.-H., et al. 2026,

Zavarygin, E. O., Webb, J. K., Dumont, V., & Riener-Sørensen, S. 2018, Mon. Not. Roy. Astron. Soc., 477, 5536, doi: [10.1093/mnras/sty1003](https://doi.org/10.1093/mnras/sty1003)

Zinchenko, I. A., Sobolenko, M., Vílchez, J. M., & Kehrig, C. 2024, A&A, 690, A28, doi: [10.1051/0004-6361/202450232](https://doi.org/10.1051/0004-6361/202450232)

Zou, H., Sui, J., Saintonge, A., et al. 2024, ApJ, 961, 173, doi: [10.3847/1538-4357/ad1409](https://doi.org/10.3847/1538-4357/ad1409)